D.A. Dei Tos, F. Topputo
Trajectory Refinement of Three-Body Orbits in the Real Solar System Model
Advances in Space Research, Vol. 59, N. 8, 2017, p. 2117-2132
doi:10.1016/j.asr.2017.01.039

Trajectory Refinement of Three-Body Orbits in the Real Solar System Model

Diogene A. Dei Tos*

Ph.D. Candidate, Department of Aerospace Science and Technology, Politecnico di Milano, Via La Masa 34, 20156, Milan, Italy.

Francesco Topputo

Assistant Professor, Department of Aerospace Science and Technology, Politecnico di Milano, Via La Masa 34, 20156, Milan, Italy.

Abstract

In this paper, an automatic algorithm for the correction of orbits in the real solar system model is described. The differential equations governing the dynamics of a massless particle in the n-body problem are written as perturbation of the circular restricted three-body problem in a non-uniformly rotating, pulsating frame by using a Lagrangian formalism. The refinement is carried out by means of a modified multiple shooting technique, and the problem is solved for a finite number of trajectory states at several time instants. The analysis involves computing the dynamical substitutes of the collinear points, as well as several Lagrange point orbits, for the the Sun–Earth, Sun–Jupiter, and Earth–Moon gravitational systems.

Keywords: n-body model, dynamical system theory, three-body problem, solar system model

1. Introduction

In the circular restricted three-body problem (CRTBP), two gravitational attractions act simultaneously upon a massless particle. The CRTBP is the easiest extension of the two-body problem, and as such it allows reproducing solutions that depart from the conics. These range from Lagrange point

*Corresponding author

Email addresses: diogenealessandro.deitos@polimi.it (Diogene A. Dei Tos), francesco.topputo@polimi.it (Francesco Topputo)

orbits (Gómez et al., 2002a) to low-energy transfers (Topputo and Belbruno, 2015). Much effort has been put to characterise the region of the phase space about the equilibrium points (Jorba and Masdemont, 1999; Gómez and Mondelo, 2001). This is because most of the dynamics in the CRTBP can be related to that of the equilibrium points. Nevertheless, large differences in both position and velocity emerge when three-body orbits are integrated in the real solar system model (Luo et al., 2014). That is, since three-body orbits are typically defined in high-sensitive regions, where the gravitational attractions tend to balance, any additional term (ascribable to eccentricity of the primaries, fourth-body perturbations, or solar radiation pressure) causes large deviations between the CRTBP orbit and the real one (Luo and Topputo, 2015). Therefore, there is the need to devise methodologies to correct the three-body orbits, while still retaining their unique features.

The dynamical substitutes of the equilibrium points and families of periodic orbits are found by continuation in energy and period in Gómez et al. (2003); Gómez and Mondelo (2001). Reduction to the centre manifold with enforcement of quasi-periodicity is performed in Gómez et al. (2002a), whereas a selection of some frequencies representing the main contributions of the solar system model is done in Gómez et al. (2002b). A large number of frequencies is instead considered in Hou and Liu (2011), where series expansion of the gravitational potential is carried out.

This paper further elaborates on an automated algorithm to refine three-body orbits in the real n-body problem, where the position of celestial bodies is modelled through precise ephemeris data. The differential equations governing the dynamics of a massless particle are written as perturbation of the CRTBP in a non-uniformly rotating and pulsating frame with a Lagrangian formalism (Gómez et al., 2002b). The refinement is carried out by means of a modified multiple shooting technique, and the problem is solved for the refined trajectory states at several locations. A finite set of NLP variables is used for the multiple shooting transcription. The obtained solution is then continued in a longer time domain through Fourier analysis and extrapolation. The generality of the algorithm lies in the possibility of handling both constrained and free boundary conditions. In the latter case, the problem is solved by minimising the correction at each step. The gradient of the objective function and the Jacobian of the constraints are computed and assembled in an automatic way. Families of halo, Lissajous, and planar Lyapunov orbits are reproduced, as well as dynamical substitutes of the Lagrange points.

The approach undertaken in this work possesses similarities with that in Lian et al. (2013) and Tang et al. (2013). Nonetheless, departures from

previous works are featured in the implementation strategy, Fourier analysis, multiple shooting scheme, and performance index definition. These peculiarities are detailed hereafter. 1) The Fourier series approach used in this work is substantially different compared to the one used by Lian et al. (2013) and addressed in Gómez et al. (2002b). The perturbing frequencies are computed as the maxima of the signals Fourier transform (positions and velocities), instead of letting them be optimisation parameters for the trigonometric polynomial search. We thus show that it is not necessary to have very precise guesses for the extrapolation step, because the modified multiple shooting algorithm is able to converge and refine those orbits even with rougher frequency information on the perturbing bodies. This accelerates the whole procedure. 2) The amplitudes of the trigonometric polynomial are found here by minimising in the least squares sense the deviation between the real trajectory and the polynomial (see Step iii). Conversely, a collocation method based on a refined Fourier analysis (described in Gómez et al. (2010a,b)) is used in Lian et al. (2013). Secondly, the algorithm is applied here to a wider range of cases. 3) Refined orbits have been computed for the Earth–Moon, Sun–Earth, and Sun–Jupiter problems. The results of the Earth–Moon problem are compared to the ones in Lian et al. (2013) and serve as solid benchmark to validate our procedure, and prove the algorithm correct and reliable. On the other hand, dynamical substitutes and refined quasi-periodic orbits of the Sun–Earth and Sun–Jupiter systems provide new scientific contribution on the subject. It is also demonstrated how the algorithm convergence properties does not depend on the particular mass ratio of the gravitational system and can be hence applied to a large variety of dynamical problems of this kind. 4) A minimisation procedure is coupled with a modified version of the multiple shooting, where the objective function is quadratic form of the defects vector. The performance index thus accounts for the displacement between the initial and final orbit, not for this difference at each iteration. This implies that all the shooting legs are considered at the same time. On the other hand, a common parallel shooting at each iteration step has been implemented in Lian et al. (2013).

The remainder of the paper is organised as follows. In Section 2 the dynamical models are described. Effort is put in deriving the solar system n-body model. Section 3 details the algorithm for trajectory refinement. This is the core of the work: emphasis is put in the methodology and numerical procedure. The results are illustrated and discussed in Section 4, whereas final remarks are drawn in Section 5.

2. Dynamics

2.1. Roto-pulsating restricted n-body problem

The equations of the solar system restricted n-body problem are written as perturbation of the CRTBP, following the derivation in Gómez et al. (2002b). This makes it easier to retain the features of orbits derived in the CRTBP, and helps understanding the corrections applied in the refinement step. We avail ourselves of the JPL ephemeris DE430 (Folkner et al., 2014) to determine in a precise way the states of the Sun, the planets, and the Moon at given epochs in an inertial reference frame centred at the solar system barycentre (SSB).

Let $\boldsymbol{r}(t)$ and $\boldsymbol{v}(t)$ be the position and velocity, respectively, of a massless particle, P, in the inertial solar system barycentric frame, and let t be the dimensional time. Let also P_1 and P_2, of masses m_1 and m_2, $m_1 > m_2$, be the two primaries of the unperturbed CRTBP, and let $\mu = m_2/(m_1 + m_2)$ be their mass ratio. The aim is writing the equations of motion for P in a roto-pulsating frame (RPF), where P_1 and P_2 are at rest (see Fig. 1). We apply the transformation

$$\mathbf{r}(t) = \mathbf{b}(t) + k(t)\mathcal{C}(t)\boldsymbol{\rho}(\tau), \tag{1}$$

where

$$\mathbf{b}(t) = \frac{m_1\mathbf{r}_1(t) + m_2\mathbf{r}_2(t)}{m_1 + m_2}, \qquad k(t) = \|\boldsymbol{r}_2(t) - \boldsymbol{r}_1(t)\|, \tag{2}$$

and $\mathcal{C}(t) = [\mathbf{e}_1(t), \mathbf{e}_2(t), \mathbf{e}_3(t)]$ is a time-dependent operator defined by

$$\begin{aligned} \mathbf{e}_1(t) &= \frac{\boldsymbol{r}_2(t) - \boldsymbol{r}_1(t)}{k(t)}, \qquad \mathbf{e}_2(t) = \mathbf{e}_3(t) \times \mathbf{e}_1(t), \\ \mathbf{e}_3(t) &= \frac{(\boldsymbol{v}_2(t) - \boldsymbol{v}_1(t)) \times (\boldsymbol{r}_2(t) - \boldsymbol{r}_1(t))}{\|(\boldsymbol{v}_2(t) - \boldsymbol{v}_1(t)) \times (\boldsymbol{r}_2(t) - \boldsymbol{r}_1(t))\|}. \end{aligned} \tag{3}$$

In Eqs. (2)–(3), $\boldsymbol{r}_1$, $\boldsymbol{r}_2$ are the position vectors of P_1, P_2 in the SSB frame, and $\boldsymbol{v}_1$, $\boldsymbol{v}_2$ are their velocities, respectively. The transformation (1) is composed by 1) a translation of the frame centre, $\mathbf{b}(t)$, from the SSB to P_1–P_2 centre of mass, 2) a rotation, $\mathcal{C}(t)$, to enforce P_1, P_2 positions on the x axis, and 3) a scaling, $k(t)$, to set P_1–P_2 distance to unity (see Gómez et al. (2001) for details). In Eq. (1), $\boldsymbol{\rho}(\tau)$ is the adimensional position vector of P in the RPF, and τ is the adimensional time given by the transformation

$$\tau = n\,(t - t_0) = \sqrt{\frac{G(m_1 + m_2)}{\bar{a}^3}}\,(t - t_0), \tag{4}$$

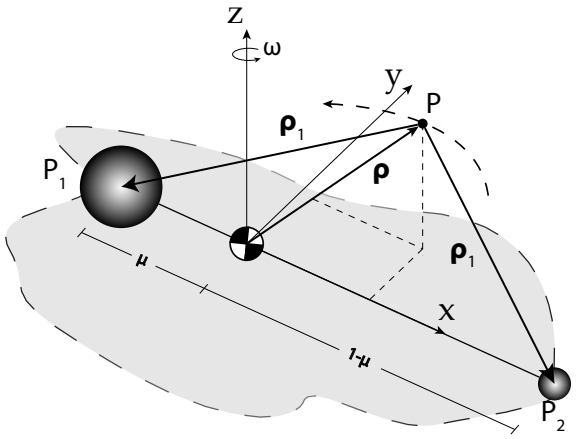

Figure 1: Roto-pulsating reference frame.

where G is the universal constant of gravitation, $\bar{a}$ is the mean P_1–P_2 distance taken for a long time interval (e.g., 400 years), and t_0 is a time shift.

The equations of motion of the roto-pulsating restricted n-body problem (RPRnBP) are obtained by plugging (1)–(4) into the Lagrangian

$$\mathscr{L}(\mathbf{r}, \dot{\mathbf{r}}, t) = T - V = \frac{1}{2}\dot{\mathbf{r}} \cdot \dot{\mathbf{r}} + \sum_{j \in \mathcal{S}} \frac{Gm_j}{\|\mathbf{r} - \mathbf{r}_j\|}, \tag{5}$$

where $\mathcal{S}$ is the set of all celestial bodies included in the solar system model and m_j are their masses. Dots indicate derivation with respect to t. Carrying out the Lagrangian mechanics operations yields the equations of RPRnBP. After some manipulations (Dei Tos, 2014):

$$\boldsymbol{\rho}'' = -\frac{2}{n}\left(\frac{\dot{k}}{k}\mathcal{I} + \mathcal{C}^T\dot{\mathcal{C}}\right)\boldsymbol{\rho}' - \frac{1}{n^2}\left[\left(\frac{\ddot{k}}{k}\mathcal{I} + 2\frac{\dot{k}}{k}\mathcal{C}^T\dot{\mathcal{C}} + \mathcal{C}^T\ddot{\mathcal{C}}\right)\boldsymbol{\rho} + \frac{1}{k}\mathcal{C}^T\ddot{\mathbf{b}}\right] + g\nabla\Omega, \tag{6}$$

where $g = G(m_1 + m_2)/(n^2k^3)$, primes indicate derivation with respect to τ, and $\nabla\Omega$ is the gradient of

$$\Omega = \frac{(1-\mu)}{\|\boldsymbol{\rho} - \boldsymbol{\rho}_1\|} + \frac{\mu}{\|\boldsymbol{\rho} - \boldsymbol{\rho}_2\|} + \sum_{j \in \mathcal{S}^*} \frac{\hat{\mu}_j}{\|\boldsymbol{\rho} - \boldsymbol{\rho}_j\|}, \tag{7}$$

with $\mathcal{S}^* = \mathcal{S}\backslash\{P_1, P_2\}$ and $\hat{\mu}_j = m_j/(m_1 + m_2)$. Mixed derivative notation in (6) acknowledges that ephemeris data is numeric, discrete, and provided for dimensional time. The vector Eq. (6) might be written per components,

$$x'' = b_1 + b_4 x' + b_5 y' + b_7 x + b_9 y + b_8 z + b_{13}\Omega_x, \tag{8a}$$
$$y'' = b_2 - b_5 x' + b_4 y' + b_6 z' - b_9 x + b_{10} y + b_{11} z + b_{13}\Omega_y, \tag{8b}$$
$$z'' = b_3 - b_6 y' + b_4 z' + b_8 x - b_{11} y + b_{12} z + b_{13}\Omega_z, \tag{8c}$$

where subscripts of Ω denote partial derivation. The model coefficients are

$$b_1 = -\frac{\ddot{\mathbf{b}}\cdot\mathbf{e}_1}{kn^2}, \quad b_2 = -\frac{\ddot{\mathbf{b}}\cdot\mathbf{e}_2}{kn^2}, \quad b_3 = -\frac{\ddot{\mathbf{b}}\cdot\mathbf{e}_3}{kn^2}, \quad b_4 = -\frac{2}{n}\frac{\dot{k}}{k},$$
$$b_5 = \frac{2}{n}\mathbf{e}_2\cdot\dot{\mathbf{e}}_1, \quad b_6 = \frac{2}{n}\mathbf{e}_3\cdot\dot{\mathbf{e}}_2, \quad b_7 = -\frac{1}{n^2}\Big(\frac{\ddot{k}}{k} - \dot{\mathbf{e}}_1\cdot\dot{\mathbf{e}}_1\Big), \quad b_8 = \frac{1}{n^2}\dot{\mathbf{e}}_1\cdot\dot{\mathbf{e}}_3,$$
$$b_9 = \frac{1}{n^2}\Big(2\frac{\dot{k}}{k}\mathbf{e}_2\cdot\dot{\mathbf{e}}_1 + \mathbf{e}_2\cdot\ddot{\mathbf{e}}_1\Big), \quad b_{10} = -\frac{1}{n^2}\Big(\frac{\ddot{k}}{k} - \dot{\mathbf{e}}_2\cdot\dot{\mathbf{e}}_2\Big),$$
$$b_{11} = \frac{1}{n^2}\Big(2\frac{\dot{k}}{k}\mathbf{e}_3\cdot\dot{\mathbf{e}}_2 + \mathbf{e}_3\cdot\ddot{\mathbf{e}}_2\Big), \quad b_{12} = -\frac{1}{n^2}\Big(\frac{\ddot{k}}{k} - \dot{\mathbf{e}}_3\cdot\dot{\mathbf{e}}_3\Big), \quad b_{13} = g.$$

2.2. Circular restricted three-body problem

The CRTBP can be reproduced as a special case of the RPRnBP. In the CRTBP the massless particle, P, is subject to the gravitational attractions of the two primaries, P_1 and P_2, which revolve in circular orbits about their centre of mass. This configuration is achieved when 1) k is constant (P_1 and P_2 in circular orbits), 2) $\mathbf{b}$ is constant (fixed centre of mass), and 3) $\mathcal{S}^* = \emptyset$ (unperturbed CRTBP). It is easy to verify that these settings produce $b_i = 0$, $i \neq \{5, 7, 10, 13\}$, $b_7 = b_{10} = b_{13} = 1$, and $b_5 = 2$. Note that $b_{13} = 1$ stems from the balance between gravitational and centrifugal forces.

We rewrite the equations of the CRTBP as (Szebehely, 1967)

$$\ddot{x} - 2\dot{y} = \Omega_x^{(3)}, \qquad \ddot{y} + 2\dot{x} = \Omega_y^{(3)}, \qquad \ddot{z} = \Omega_z^{(3)}, \tag{9}$$

where the three-body potential function can be expressed as

$$\Omega^{(3)} = \frac{1}{2}(x^2 + y^2) + \frac{1-\mu}{r_1} + \frac{\mu}{r_2} + \frac{1}{2}\mu(1-\mu), \tag{10}$$

and $r_1 = \sqrt{(x+\mu)^2 + y^2 + z^2}$, $r_2 = \sqrt{(x-1+\mu)^2 + y^2 + z^2}$. Eqs. (9) consider the distance between primaries, their angular speed, and the sum of their masses all equal to one. Moreover, P_1 and P_2 are located at $(-\mu, 0, 0)$ and $(1-\mu, 0, 0)$, respectively.

The CRTBP possesses five equilibrium points, three of them located along the x axis (collinear points), and the others at the vertex of two equilateral triangles having the primaries distance as common base (triangular points). Table 1 displays the location of the collinear points for three models considered in the present work.

Table 1: Mass parameters and location of collinear points for the systems considered.

System		Mass ratio	Collinear points		
P_1	P_2	μ	L_1	L_2	L_3+1
Sun	Jupiter	9.53881157e-4	0.93236545	1.06883066	-3.97450e-4
Sun	Earth	3.00348059e-6	0.99002659	1.01003412	-1.25145e-6
Earth	Moon	1.21505843e-2	0.83691513	1.15568226	-5.06264e-3

3. Methodology

3.1. Statement of the problem

Let $\boldsymbol{\varphi}_{nb}(\boldsymbol{x}_0, t_0; t)$ be the solution at time t of Eqs. (8) starting from $(\boldsymbol{x}_0, t_0)$, and let $\gamma_{nb}(\boldsymbol{x}_0) = \{\boldsymbol{\varphi}_{nb}(\boldsymbol{x}_0, t_0; t)\ \forall t \geq t_0\}$ be the related orbit. Analogously, let $\boldsymbol{\varphi}_{3b}(\boldsymbol{x}_0, t_0; t)$ and $\gamma_{3b}(\boldsymbol{x}_0)$ denote the flow and orbit of Eqs. (9), respectively. By definition, γ_{nb} and γ_{3b} are different. The extent of this difference may depend upon the eccentricity of P_1 and P_2, the number of bodies in $\mathcal{S}^*$, and ultimately on t_0 and $\boldsymbol{x}_0$. This divergence might be further favoured by the chaotic nature of the problem at hand: within the same model (CRTBP or RPRnBP) orbits are already sensitive to small variations in the initial conditions and model parameters.

The CRTBP allows designing orbits of practical interest related to the dynamics about the Lagrange points, yet the real-world motion is described by the RPRnBP. There is then the need to refine three-body orbits into the RPRnBP. However, since the CRTBP orbits are unique, their features shall be preserved. The methodology, and ultimately the algorithm designed in this work, has the primary objective to aid the transition between: a) orbits designed within simplified models, and b) the real n-body world. By simplified model we mean the CRTBP, but also the elliptic restricted three-body problem (ERTBP), the bicircular restricted four-body model (RFBP), and any other simplification of the dynamics at hand (i. e., Hill approximation). This is a step that is of paramount importance in the process of trajectory design for two reasons:

1. the feasibility assessment of flying such orbits, failure probability checks, the transfer navigation analysis, the precise manoeuvres scheduling and actuation, the generation of top level requirements on ground systems, and essentially most of the mission operation phases must be studied, tested and validated in the real dynamics, that is the solar system n-body dynamics;

2. the mission will eventually have to fly in the real scenario, thus the nominal trajectory is by definition the one that exists in the real solar system model.

In mathematical terms, our problem can be thus stated as follows.

Problem. Find a modified initial condition, $\hat{\boldsymbol{x}}_0$, such that $\gamma_{nb}(\hat{\boldsymbol{x}}_0)$ retains the dynamical (frequency content) and geometrical (orbital region) features of $\gamma_{3b}(\boldsymbol{x}_0)$. In particular, if $\gamma_{3b}(\boldsymbol{x}_0)$ is an equilibrium point of the CRTBP, $\boldsymbol{x}_0$ shall be corrected into $\hat{\boldsymbol{x}}_0$ such that $\gamma_{nb}(\hat{\boldsymbol{x}}_0)$ is the dynamical substitute of the equilibrium point. Similarly, if $\gamma_{3b}(\boldsymbol{x}_0)$ is a periodic orbit, $\gamma_{nb}(\hat{\boldsymbol{x}}_0)$ shall be a quasi-periodic orbit with similar amplitude and harmonic content as $\gamma_{3b}(\boldsymbol{x}_0)$.

The methodology developed to tackle this problem is based on three parts:

1. Generation of an initial seed orbit;
2. Correction with modified multiple shooting;
3. Interpolation/extrapolation by Fourier analysis.

In Part 1, an initial seed orbit is generated. This can be either a CRTBP orbit (at iteration zero) or an orbit resulting from Part 3. In Part 2, the correction from CRTBP to RPRnBP is implemented via a modified multiple shooting scheme. This is an iterative method (inner loop) that solves a Two-Point Boundary Value Problem (TPBVP) with minimal corrections at each step. In Part 3, a Fourier analysis is carried out. This is used either to have a denser grid (interpolation) or to widen the time span (extrapolation). The overall procedure above is iterative: time spans are progressively increased until a desired duration is covered (Lian et al., 2013).

3.2. The modified multiple shooting

A TPBVP (Armellin and Topputo, 2006) consists in finding $\mathbf{x}(t)$, $t \in [t_0, t_f]$, such that

$$\dot{\mathbf{x}} = \mathbf{f}(\mathbf{x}, t), \qquad \mathbf{h}(\mathbf{x}(t_0), \mathbf{x}(t_f)) = \mathbf{0}. \tag{11}$$

In the present context, the first equation is the state space representation of Eqs. (8) ($\boldsymbol{x}$ is 6-dimensional); the function $\mathbf{h}$ specifies six boundary conditions, which are needed to well-pose the problem (Bolle and Circi, 2012). In multiple shooting, problem (11) is solved for a finite set of variables (Mingotti et al., 2012). The procedure is briefly recalled here for convenience.

The solution is discretised over m grid points $t_0 = t_1 < t_2 < \cdots < t_m = t_f$; that is, $\mathbf{s}_k = \mathbf{x}(t_k)$, $k = 1, \ldots, m$. This defines $m-1$ segments in which a TPBVP is solved by enforcing continuity of the solutions at both ends. This shortens the duration of the original problem, and thus reduces sensitivity. Let the defect vector be

$$\boldsymbol{\zeta}_k = \boldsymbol{\varphi}_{nb}(\mathbf{s}_k, t_k; t_{k+1}) - \mathbf{s}_{k+1}, \quad k = 1, \ldots, m-1. \tag{12}$$

The problem is to determine the states $\mathbf{s}_k$ such that

$$\mathbf{h}(\mathbf{s}_1, \mathbf{s}_m) = \mathbf{0}, \quad \text{and} \quad \boldsymbol{\zeta}_k = \mathbf{0}, \quad k = 1, \ldots, m-1. \tag{13}$$

In Eqs. (13) we have $6m$ unknowns (the states $\mathbf{s}_k$) and $6m$ equations (6 boundary conditions and $6(m-1)$ defect constraints). This is the classic multiple shooting method.

Hereafter the multiple shooting is modified to deal with free boundary conditions. That is, the technique has to cope with the fact that no boundary conditions are actually known (e.g., periodicity cannot be enforced in the RPRnBP), and the sole requirement is to produce a continuous trajectory that stays as close as possible to the initial seed. The problem cast in this way possesses $6m$ degrees of freedom, and thus an optimisation procedure is implemented to provide the 6 missing equations (Topputo, 2013).

Let $\mathbf{s} = (\mathbf{s}_1, \mathbf{s}_2, \ldots, \mathbf{s}_m)$ be the vector of unknowns and let

$$\mathbf{c}(\mathbf{s}) = (\boldsymbol{\zeta}_1(\mathbf{s}_1, \mathbf{s}_2), \boldsymbol{\zeta}_2(\mathbf{s}_2, \mathbf{s}_3), \ldots, \boldsymbol{\zeta}_{m-1}(\mathbf{s}_{m-1}, \mathbf{s}_m)) \tag{14}$$

be the vector of defects. The zero of the function $\mathbf{c}(\mathbf{s})$ is sought while minimising a scalar objective function $f(\mathbf{s})$, which is defined later. The problem is then stated as

$$\min_{\mathbf{s}} f(\mathbf{s}) \quad \text{subject to} \quad \mathbf{c}(\mathbf{s}) = \mathbf{0}. \tag{15}$$

From the theory of Nonlinear Programming (Betts, 2010), problem (15) is solved by finding the conditions that extremise the Lagrangian

$$\mathscr{L}(\mathbf{s}, \boldsymbol{\lambda}) = f(\mathbf{s}) + \boldsymbol{\lambda} \cdot \mathbf{c}(\mathbf{s}), \tag{16}$$

where $\boldsymbol{\lambda}$ is the $6(m-1)$-dimensional vector of multipliers. Necessary conditions for a minimum of $\mathscr{L}$ are

$$\nabla_{\mathbf{s}} \mathscr{L} = \mathbf{g} + \mathcal{J}_c^T \boldsymbol{\lambda} = \mathbf{0}, \qquad \nabla_{\boldsymbol{\lambda}} \mathscr{L} = \mathbf{c} = \mathbf{0}, \tag{17}$$

where $\mathbf{g}$ is the gradient of the objective function, $\mathbf{g} = \nabla_{\mathbf{s}} f(\mathbf{s})$, $\mathcal{J}_c$ is the Jacobian of $\mathbf{c}$,

$$\mathcal{J}_c(\mathbf{s}) = \begin{bmatrix} \Phi_1 & -\mathcal{I} & 0 & & 0 \\ 0 & \Phi_2 & -\mathcal{I} & \ddots & \\ & \ddots & \ddots & \ddots & 0 \\ 0 & & \ddots & \Phi_{m-1} & -\mathcal{I} \end{bmatrix}, \tag{18}$$

and $\Phi_k = \nabla_{\mathbf{s}_k} \boldsymbol{\varphi}(\mathbf{s}_k, t_k; t_{k+1})$ is the state transition matrix, $k = 1, \ldots, m-1$.

System (17) has to be solved for $(\mathbf{s}, \boldsymbol{\lambda})$. Once an initial guess is provided, $(\mathbf{s}^{(0)}, \boldsymbol{\lambda}^{(0)})$, applying Newton's method leads to solving iteratively

$$\begin{bmatrix} \mathcal{H}_{\mathscr{L}} & \mathcal{J}_c^T \\ \mathcal{J}_c & 0 \end{bmatrix} \begin{pmatrix} \mathbf{s}^{(i+1)} - \mathbf{s}^{(i)} \\ \boldsymbol{\lambda}^{(i+1)} \end{pmatrix} + \begin{pmatrix} \mathbf{g}(\mathbf{s}^{(i)}) \\ \mathbf{c}(\mathbf{s}^{(i)}) \end{pmatrix} = \mathbf{0}, \tag{19}$$

where the superscript indicate iterations, and $\mathcal{H}_{\mathscr{L}}$ is the Hessian:

$$\mathcal{H}_{\mathscr{L}} = \nabla_{\mathbf{s}}(\mathbf{g} + \mathcal{J}_{\mathbf{c}}^T \boldsymbol{\lambda}) = \nabla_{\mathbf{s}}^2 f + \sum_{i=1}^{m-1} \lambda_i \nabla_{\mathbf{s}}^2 c_i. \tag{20}$$

Eqs. (19) are used to solve Problem described in Section 3.1. Enforcing γ_{nb} to retain the characteristics of the initial CRTBP seed means minimising the corrections applied by the modified multiple shooting. This is done by choosing the cost function f to be a quadratic form of the constraints, i.e.,

$$f(\mathbf{s}) = \frac{1}{2} \mathbf{c} \cdot \mathcal{M} \mathbf{c}, \tag{21}$$

where $\mathcal{M}$ (positive-defined matrix) weighs the components of the state.

3.3. Fourier interpolation and extrapolation

Ultimately, the Fourier analysis provides a powerful tool to approximate a quasi-periodic function by means of the trigonometric series

$$Q(t) = A_0 + \sum_{k=1}^{N_f} \left(A_k \cos \frac{2\pi f_k t}{T} + B_k \sin \frac{2\pi f_k t}{T} \right), \tag{22}$$

where $\{A_k\}_{k=0}^{N_f}$, $\{B_k\}_{k=1}^{N_f}$ are the $2N_f+1$ interpolating coefficients, $\{f_k\}_{k=1}^{N_f}$ is the set of N_f frequencies to be retained, and T is the time interval amplitude.

In this work an extrapolation becomes necessary in order to provide the multiple shooting algorithm with a consistent initial guess when the time interval is progressively increased. The interpolation/extrapolation is applied component-wise to the state vector (i. e., six times). Without loss of generality, in the remainder the sole x component is considered. Given N samples $x_j = x(t_j)$ at discrete distinct times $t_j \in [0, T]$, find the polynomial $Q(t)$ that best approximates the real-valued quasi-periodic function $x(t)$. The procedure consists of four steps:

(i) Fix the number of frequencies, N_f;
(ii) Calculate the retained frequencies, f_k, as the maxima of the Fourier transform magnitude;
(iii) Compute the trigonometric amplitudes, A_k and B_k, through an unconstrained optimisation;
(iv) Evaluate the interpolating polynomial over a larger time domain.

Step (i) is straightforward, based on several simulations we set $N_f = 4$. In fact, this is a lower bound because the number of retained frequencies is increased iteratively (maximum 13), until a tolerance in Step (iii) is met. The maximum number of retained frequencies has been fixed equal to 13 after some numerical experiments. There is evidence that beyond this point there is no significant improvement in the interpolated trajectory for all cases analysed in this study. In other terms, the multiple shooting was able to attain convergence for all cases in which N_f has reached values greater (or equal) than 13. This should not surprise, because there are typically no more than 10 independent values of the parameters for the best Fourier analysis of the coordinates of the solar system bodies in the roto-pulsating frame, as shown in Table 5 of Gómez et al. (2002b) for the Earth-Moon system (this is true also for the Sun–Jupiter and Sun–Earth systems).

Let $F_x(f)$ be the Fourier transform[1] of $\hat{x}(t)$; the frequencies f_k are then calculated in Step (ii) as maxima of the Fourier transform magnitude as

$$f_k \mid F_x(f_k) = \max |F_x(f)| \quad \text{for } k = 1, \ldots, N_f. \tag{23}$$

To obtain $\hat{x}(t)$, the function $x(t)$ is modified such that 1) it's centred at the libration point, in order to delete a fix bias in the input signal; 2) 10% of points are removed from each end of the vector to limit any spurious harmonic content due to the free boundaries; and 3) it is filtered with a second order Hanning window function, $H_T^2(t) = 2/3[1 - \cos(2\pi t/T)]^2$, to

[1] The Fourier transform is computed by means of the Matlab's FFT algorithm.

reduce the leakage effect (Gómez et al., 2002b). Because of the discrete nature of the samples, two additional topological conditions must be verified: x_j has to be equally spaced in time, and it must contain a minimum number of points (depending on the maximum frequency to be resolved and on the size of the time domain), N_{min}, to avoid aliasing. A denser grid is generated by interpolation if the latter requirement is not satisfied. The integration scheme is applied and then the outputs are interpolated at given time instants.

In Step (iii) the trigonometric polynomial amplitudes are found by minimising the mean square deviation between $Q(t)$ and $x(t)$:

$$\min_{A_k,B_k} \frac{1}{N} \sum_{j=1}^{N} \Big(x(t_j) - Q(t_j) \Big)^2. \tag{24}$$

Even though the interpolating polynomial is not necessarily equal to the real trajectory at any sampling time, this strategy has been preferred to a control point scheme because of the large difference between degrees of freedom and samples number, $N \gg 2N_f + 1$. Fig. 2 shows an application of this technique on a simple disturbed sinusoid signal.

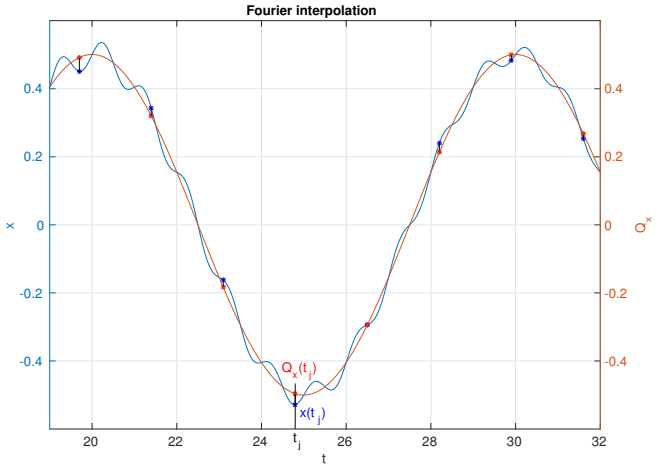

Figure 2: Fourier interpolation on $x(t) = 0.5\cos(2\pi f_1 t) + 0.1\sin(2\pi f_2 t)\exp(-3.5t/T)$, with $f_1 = 0.1$ Hz, $f_2 = 1$ Hz. The maximum of the Fourier transform is at 0.099 Hz, and the optimisation is carried out for this single frequency. The resulting objective function is $J = 7e{-}4$ on equally-spaced points. The control points are shown to graphically represent how the objective function is computed.

Finally, the extrapolation of a new initial guess for the refinement proce-

dure is performed in Step (iv) by evaluating $Q(t)$ over a larger time domain:

$$x^{(i+1)}(\bar{t}) = Q^{(i)}(\bar{t}) \quad \text{where} \quad \bar{t} \in [0, T + \Delta T], \tag{25}$$

where superscript indicates steps in the refinement procedure.

The use of the Fourier transform theory to extrapolate the trajectory is justified by numerical experiments. In the orbits of interest, the components of the state vector oscillate about equilibrium values that are in general defined in the framework of the CRTBP. The dynamics and shape of the oscillations depend on the relative strength of the perturbation, if compared to the CRTBP gravitational effects. In this work, single component interpolation has been preferred to dedicated three-dimensional interpolating techniques for position and velocity vectors. Although the latter makes more sense from the physical perspective, it does not significantly improve the algorithm performances, neither the speed-up of the interpolation/extrapolation step.

3.4. Summary of the algorithm

A more detailed description of the whole iterative procedure requires the introduction of some notation. Let T_0 be the initial epoch, which should be specified due to the nonautonomous nature of the n-body problem, ΔT the time-span covered by a certain set of nodes, ΔT_0 the time-span considered for the initial guess provided by the CRTBP, and ΔT^* the final time-span desired. N denotes the number of nodes, and N_{min} the minimum number of nodes required by the Fourier analysis to be consistent. During the process, a factor γ_P is used to enlarge ΔT at each step, $\Delta T^{(i+1)} = \gamma_P \Delta T^{(i)}$. The basic procedure for trajectories refinement in the n-body problem is shown as flowchart in Fig. 3 and consists basically of the following steps.

Step 1 Generate a sequence of nodes as initial guess, $\boldsymbol{x}_0$, within the CRTBP for *Step 2*;

Step 2 Fix the initial epoch, T_0, and for a given time span ΔT, perform the modified multiple shooting starting from $\boldsymbol{x}_0$;

Step 3 If $N < N_{min}$, do a denser sampling using the sequence of nodes obtained in *Step 2* by numerical piecewise integration;

Step 4 At both ends of the resulting sequence, remove 10% of the nodes to cope with the fact that no boundary conditions are specified;

Step 5 Perform the Fourier analysis of the six state components of the trajectory computed in *Step 4*. With the set of basic frequencies, $\{f_k\}_{k=1}^{N_f}$, compute the amplitudes of the trigonometric approximation polynomial of the orbit by means of the optimisation in Eq. (24);

Step 6 Check the total time span condition: if $\Delta T \geq \Delta T^*$, go to *Step 8*, otherwise, go to *Step 7*;

Step 7 Extrapolate the new set of nodes as initial guess for a larger time span, $\Delta T = \gamma_P \Delta T$, $\gamma_P > 1$, using the trigonometric polynomials computed in *Step 5*; then go to *Step 2*;

Step 8 Stop.

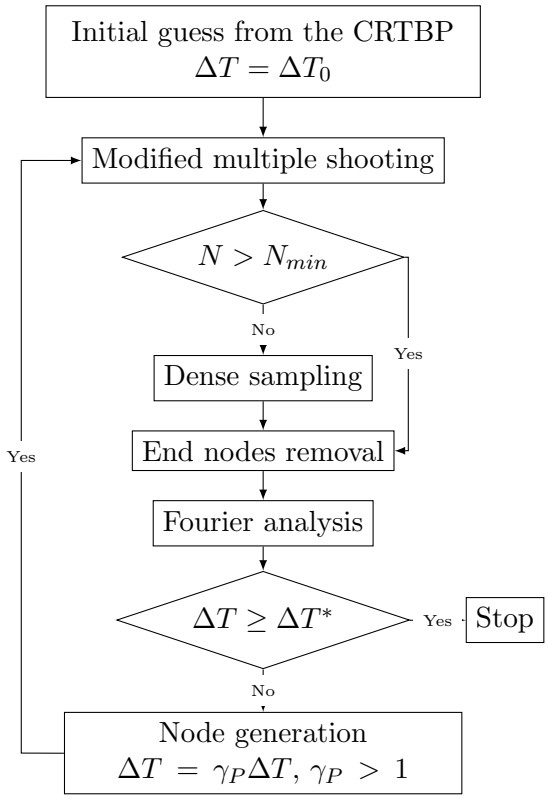

Figure 3: Flowchart of the iterative algorithm for orbit refinement.

Numerical implementation. All data processing and implementations were performed using the commercial software Matlab. Serial calculations have been carried out on a MacBookPro 2.9 GHz Intel Core i7 with 8 Gb of RAM; whilst a hub of 64 (20 at 1400 MHz and 44 at 2300 MHz) AMD Opteron^{TM} Processors 6376 with 264 Gb of RAM[1] ran the parallel computations. The following are the main numerical features of the algorithms used for the trajectories refinement.

- Chebyshev polynomial interpolation is used to get precise celestial bodies state at specified epochs from DE430 JPL ephemeris[2];
- Numerical integrations are performed with the suite *ode113* (Shampine and Reichelt, 1997), which implements a variable order, adaptive multistep Adams–Bashforth–Moulton method in a PECE[3] mode (predict, evaluate, correct, evaluate). Both absolute and relative error tolerances have been set to $3 \cdot 10^{-14}$.
- The state transition matrices, Φ_k, have been calculated by means of a forward finite-difference scheme, the driving factor for this choice being the computational time. The small perturbation magnitude has been set to $\delta = (|s| + 1)\sqrt{\texttt{eps}}$, where s is the state component with respect to which differentiation is carried out and `eps` is the smallest floating point number.
- The optimisation has been carried out by means of the Matlab built-in function *fmincon*, exploiting the interior-point algorithm; the multiple shooting procedure is performed in a parallel fashion, due to its high computational demand.

4. Results

4.1. Dynamical substitutes of collinear points

The solar system restricted n-body equations of motion are nonautonomous, and therefore there are no relative equilibrium points in this model.

[1] This is the Copernicus workstation at the Department of Aerospace Science and Technology, Politecnico di Milano.

[2] The JPL planetary and lunar ephemerides are available via a secure ftp server on the NASA and JPL ports at `ftp://ssd.jpl.nasa.gov/pub/eph/planets/ascii/`.

[3] The ABM method uses the explicit Adams–Bashforth method as predictor, and the implicit Adams–Moulton method as corrector.

The combined effects of the major solar system bodies, as well as the generally elliptical motion of the primaries, prevent the Lagrangian points to be relative equilibria. Nevertheless, when proper initial conditions are flown under the n-body dynamics, special trajectories arise, that can be interpreted as dynamically substituting the libration points of the CRTBP. In this sense, the dynamical substitutes of the equilibrium points are defined as those solutions of the equations of motion that have as basic frequencies only those of the perturbing bodies, while still remaining about the CRTBP equilibria.

Using the numerical method described in the previous section, dynamical substitutes of the three collinear libration points for the Sun–Jupiter, Earth–Moon and Sun–Earth systems are computed. It must be remarked that, for each point, these substitutes are not unique since they depend, for instance, on the initial epoch at which they are computed. The initial epoch has been fixed to MJD 0 in this paper (0h UT on January 1, 2000), and for all the refinement procedures. The initial seeds used for the procedure are the three equilibrium points of the CRTBP along a certain time interval. Dynamical substitutes of the Sun–Jupiter collinear points have been calculated for 150 years; Earth–Moon ones for 5 years; and Sun–Earth's for a period of 20 years. This choice follows from rough considerations on the primaries dynamics. In particular, timespans have been selected that cover most of the relevant Sun–Jupiter, Earth–Moon, or Sun–Earth periods, respectively. The Fourier analysis for the trigonometric approximation and extrapolation polynomial was necessary, and has been used, only in the Sun–Earth case. Indeed, this turned out to be the most difficult case the algorithm has handled, due to the relatively high perturbation of the Moon. The dynamics of Sun–Earth Lagrangian point orbits is indeed greatly affected by the presence of the Moon which modifies the phase space of this region due to its vicinity. Furthermore, the Moon features a fast dynamics and introduces in the RPRnBP high frequency terms which affect both dynamical substitutes and quasi-periodic refined solutions. In this case, to attain the convergence of the method and in order to span a large time interval, the procedure has been started with $\Delta T_0 = 2$ years, $\Delta T^* = 20$ years, and $\gamma_P = 1.5$.

The resulting orbits are shown in Figs. 4–6 for Sun–Jupiter, Earth–Moon and Sun–Earth systems, respectively. The figures display dimensional coordinates in the RPF. For the sake of clarity, and due to the large amount of data, only the first 10 segments are shown, where a segment corresponds to the primary revolution period (i. e., roughly 110 years for Sun–Jupiter, 1 year for Earth–Moon, and 10 years for Sun–Earth). These results are in agreement with those obtained in Gómez et al. (2002b); Hou and Liu

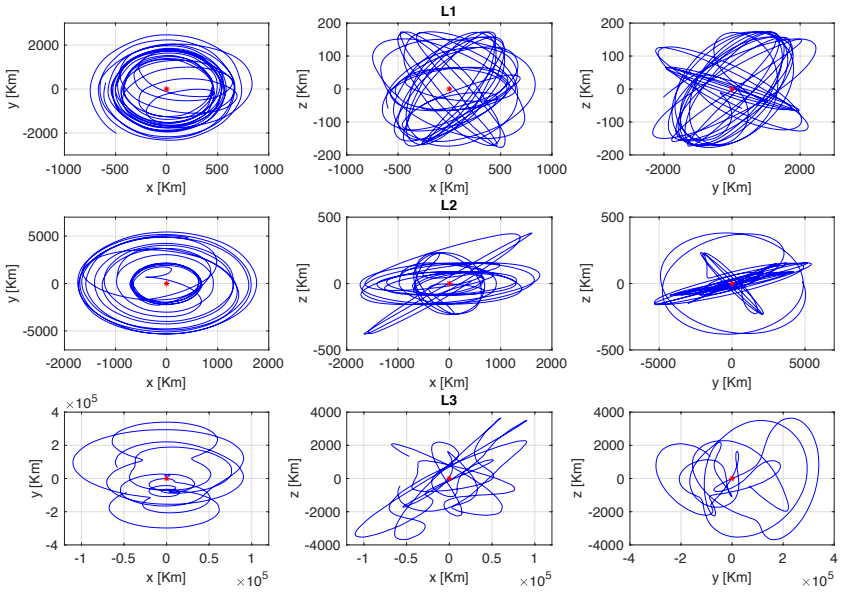

Figure 4: Dimensional coordinate projections of the dynamical substitutes of the L_1 (top), L_2 (middle), and L_3 (bottom) of the Sun–Jupiter system in the real ephemeris n-body dynamics (only the first 110 years of the computed orbits are displayed).

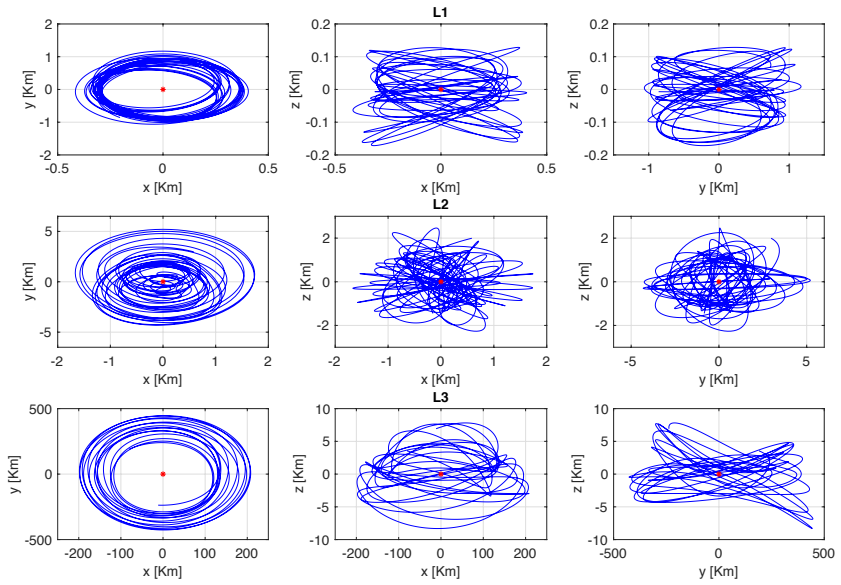

Figure 5: Dimensional coordinate projections of the dynamical substitutes of the L_1 (top), L_2 (middle), and L_3 (bottom) of the Earth–Moon system in the real ephemeris dynamics (1 year of computed orbits is displayed).

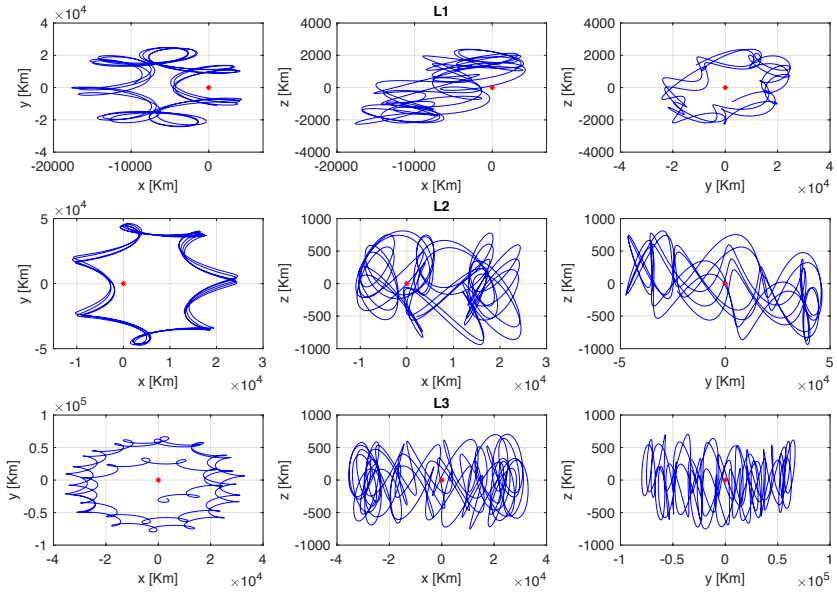

Figure 6: Dimensional coordinate projections of the dynamical substitutes of the L_1 (top), L_2 (middle), and L_3 (bottom) of the Sun–Earth system in the real ephemeris n-body dynamics (only the first 10 years of the computed orbits are displayed).

(2011); Lian et al. (2013) by means of other methods. As can be seen in Figures 4–6, the sizes of the dynamical substitutes orbits are relatively small if compared to the mean distance between the primaries. An exception is the dynamical substitutes of the Sun–Earth system, which orbit at tens of thousands of kilometres about the collinear points. This is probably due to the fact that the Sun–Earth gravitational system has been considered, instead of the Sun–(Earth+Moon) model. Table 2 displays the amplitude of such orbits for each gravitational system and discriminating for the collinear libration points. There is a patent increase of the dynamical substitute orbit amplitude along with the decrease of Jacobi constant; that is, the orbit is larger for higher energy content.

Table 2: Approximate amplitude [km] of dynamical substitutes orbits.

	Sun–Jupiter	Earth–Moon	Sun–Earth
L_1	6.137127e+3	0.6286745	1.5918748e+4
L_2	12.561253e+3	2.0198146	3.0544518e+4
L_3	634.893168e+3	240.7262349	4.390072e+4

As far as the Earth–Moon case is concerned, though smaller, the orbit of L_1 moves in a more regular way (a torus-like shape) than the substitutes of L_2, which in some sense reflects the fact that dynamics around L_2 point is more rich and complex. Quite the contrary, the totality of Sun–Jupiter dynamical substitutes reveal a high chaotic behaviour, in particular the path around L_2 manifests the tendency to change orbital plane periodically. Last but not least, the Sun–Earth dynamical substitutes, relatively the largest in amplitude, show a clear-cut quasi-periodic behaviour. The gravitational system analysed in this work have been carefully selected. Indeed, the Sun–Jupiter represents a good example low-perturbed gravitational system, whereas the Sun–Earth system is a good example of higher perturbations in the dynamics (mainly due to the Moon and Jupiter). Lastly, The Earth–Moon represents a system with larger gravitational mass ratio, large perturbations due to the Sun, and high frequency content due do its faster angular rotation when compared to the other main planets in our solar system.

The Fourier transform of the x component of the Earth–Moon L_3 dynamical substitute is shown in Fig. 7. The largest contributions, at 0.9176 and 1.9270 adimensional frequencies, are ascribable to the Sun perturbation (see Table 6 in Gómez et al. (2002b)).

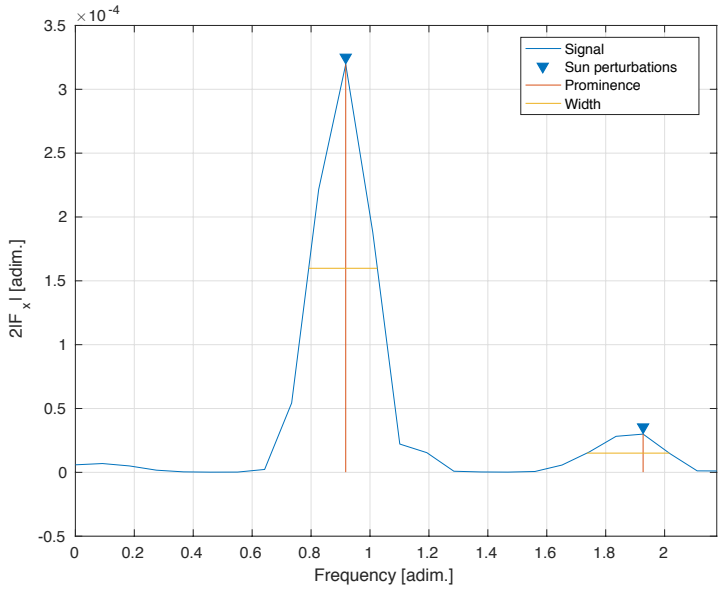

Figure 7: Fourier transform of the Earth–Moon L_3 dynamical substitute, x component.

The refinement algorithm eventually reintegrates the output trajectory to check if consistency is attained with respect the piecewise solution. It happened in the course of simulations, that the specified tolerance was either too strict, or too loose. The effect was either a very slow, if at all, convergence, or errors in the dynamics that, propagated forward, gave rise to an orbit detaching the sought solution and allowed the massless particle to move far away from the libration point, according to its Jacobi energy. Another possible cause of error is the vicinity of the orbit to a bifurcation phenomenon, ascribable for instance to the bifurcation of planar Lyapunov orbit to the halo family. In rare cases, during the iterations the algorithm has 'jumped' between the two possible options and ended up refining a different kind of orbit. This occurrence should not surprise, in fact also differential corrections in the framework of CRTBP might produce a planar Lyapunov orbit when seeking a small-amplitude halo one. Lastly, errors might come from the overfitting of the data if the Fourier analysis and extrapolation are done with very restrictive constraints. Namely, the approximated polynomial will perfectly fit the discrete vector in the given domain, but will have exponential increasing error for small displacement from the nominal domain when extrapolating.

4.2. Periodic orbits

This section is devoted to the refinement of periodic orbits around both L_1 and L_2 of the Sun–Jupiter, Earth–Moon and Sun–Earth gravitational systems; which include halo, Lissajous, and planar Lyapunov orbits. In this work the seeding orbits necessary to start the algorithm are calculated via a third-order analytic first guess that is differentially corrected by means of a *Lindstedt-Poincaré method* (Richardson, 1980) for the halo and Lyapunov cases; while CRTBP linearised solutions are used as seeding for the Lissajous orbits.

4.2.1. The halo family

Due to the symmetry of the CRTBP with respect to the xy plane, there appear two families of halo orbits at the bifurcation. In the following, the northern[1] family orbits are refined in the n-body problem. Halo orbits can be characterised by an amplitude parameter, A_z. Different values of A_z univocally correspond to different energy levels, and thus to different values of the Jacobi constant, C_J. Hence, given any of these two parameters, one particular halo orbit is specified. Fig. 8 displays the refinement of three halo

[1]Maximum z-amplitude along the positive z direction.

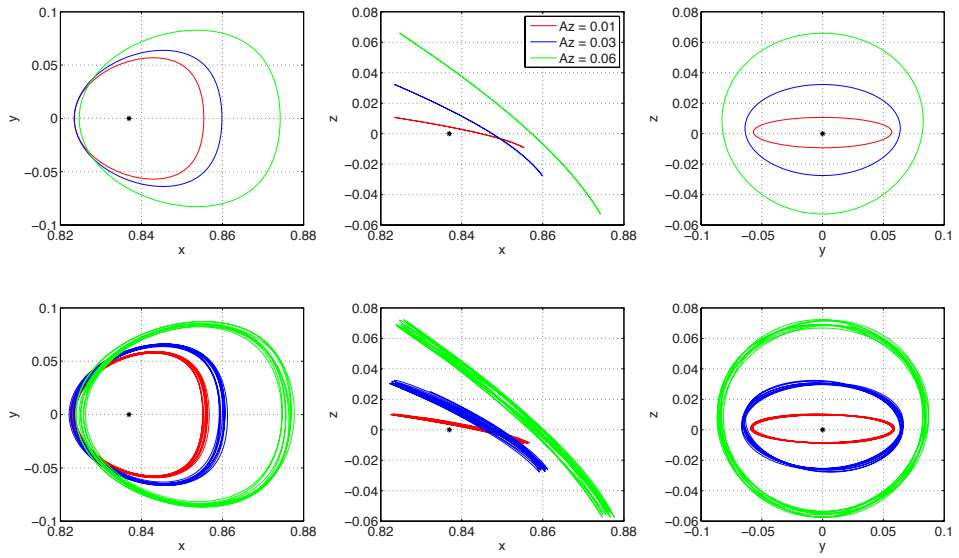

Figure 8: Initial CRTBP guess (top) and refinement (bottom) of halo orbits with $A_z = 0.01$ (smallest orbit), $A_z = 0.03$, and $A_z = 0.06$ (largest orbit) of the Earth–Moon L_1 libration point. Only the first year is plotted here.

orbits about the Earth–Moon L_1, associated to three different amplitudes, $A_z = 0.01, 0.03, 0.06$. Note that larger amplitude means larger orbital path, and therefore smaller Jacobi energy, C_J. The refinement has been done for 4 years, but for the sake of presentation clarity, only the first year is graphed. Fig. 9 shows a three-dimensional view of the refinement operated on two halo orbits about L_1 and L_2 of Sun–Jupiter system, for a period of 50 years. Both the CRTBP halo seeds have been calculated with a fixed amplitude of $A_z = 0.01$. Finally, in Fig. 10, two halo orbits about the Sun–Earth L_2 point are considered, whose amplitudes are $A_z = 0.002$ and $A_z = 0.005$. From the obtained results and the presented figures, it is clear that the numerical refinement procedure of a halo orbit produces a quasi-periodic one, where the baseline shape and size are retained.

A Fourier analysis of the refined halo-type orbit about Sun–Earth L_2, whose x component is depicted in Fig. 11, shows that the main single halo frequency is maintained. In addition, since the refined orbit is now quasi-periodic, other frequencies appear. In particular, the frequency corresponding to Mercury and the Moon are highlighted. Note that the perturbative effects of other massive planets are present, but cannot be resolved by the Fourier transform due to the limited total period (11 years).

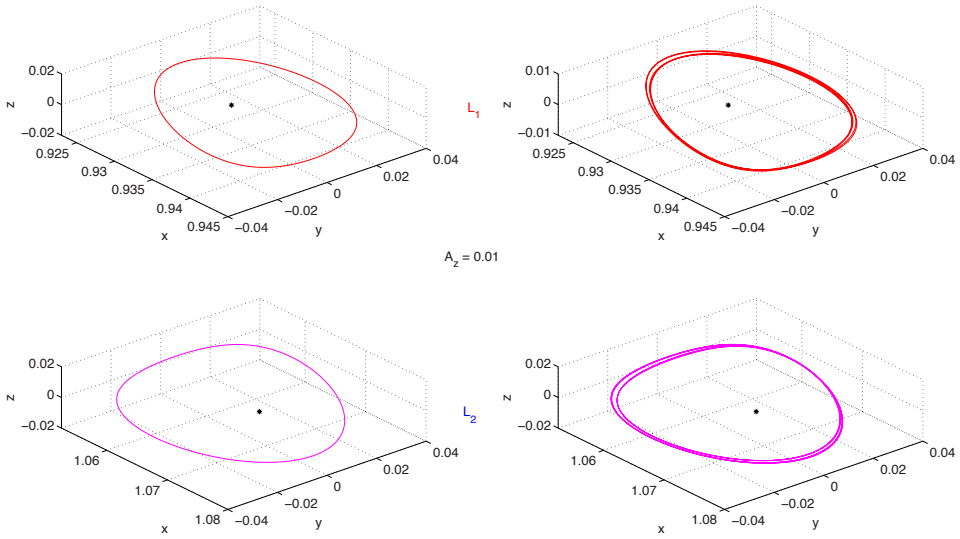

Figure 9: Halo orbits ($A_z = 0.01$) and their numerical 50-year refinements around L_1 (top) and L_2 (bottom) of the Sun–Jupiter system. Left hand side: CRTBP orbits; right hand side: refined orbits.

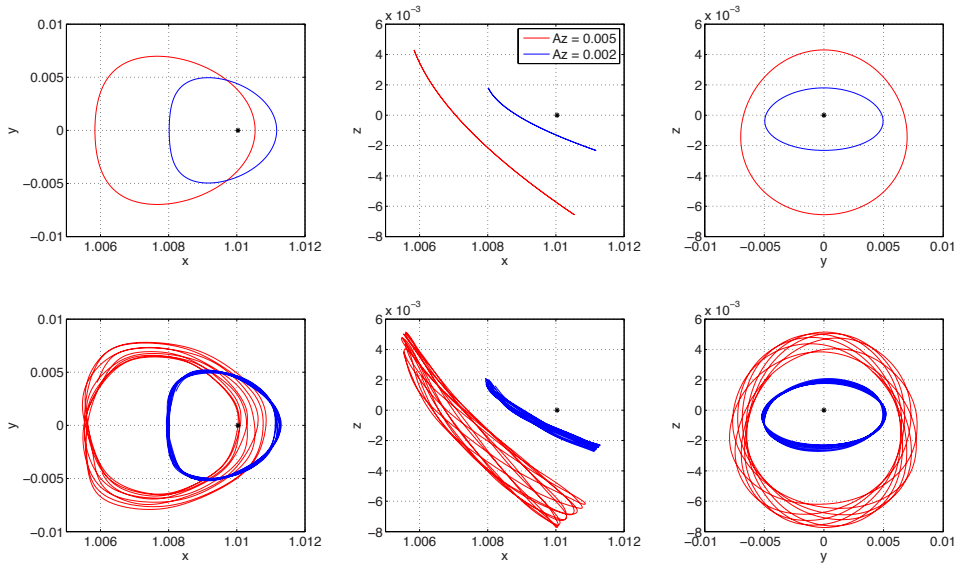

Figure 10: Initial CRTBP guess (top) and refinement (bottom) of halo orbits with $A_z = 0.002$ (smallest orbit), and $A_z = 0.005$ (largest orbit) of the Sun–Earth L_2 collinear point. 11 years are plotted here.

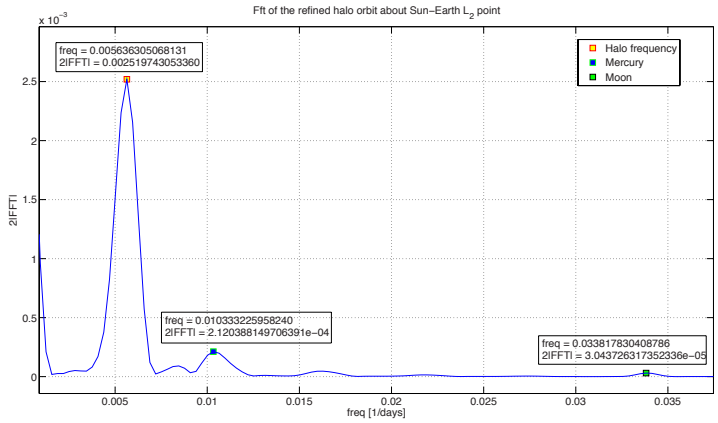

Figure 11: Fourier transform of the $A_z = 0.01$ halo orbit abut the L_2 of Sun–Earth gravitational system, x component.

There is a common trend that the frequencies follow when the time domain is progressively increased. For shorter amount of time the frequencies corresponding to the maxima of the Fourier transform span the whole available spectrum because there is typically one high peak, if compared to the others that are more spread out and with similar values. These frequencies tend to absorb part of the signal captured later on by other frequencies when the time domain is increased. Specifically, when the time domain is increased clearer and well-separated peaks appear; the chosen frequencies assume then values that concentrate around those peaks and provide a better picture of the harmonic content of the refined orbit dynamics. Fig. 12 shows this trend.

4.2.2. The Lissajous family

Lissajous orbits appear in the linearised CRTBP when the stable and unstable parts of the central manifold are set to zero (Alessi et al., 2010). These orbits feature different in-plane and out-of-plane frequencies, that solely depend on the primaries and on the Lagrange point selection. For the collinear points at x_{L_j}, the square of the Lissajous frequencies simply yield:

$$\lambda = \sqrt{c_2\Big(\frac{9}{4}c_2 - 2\Big)} - \Big(\frac{c_2}{2} - 1\Big), \quad c_2 = |x_{L_j} + \mu|^3 + |x_{L_j} - 1 + \mu|^3. \quad (26)$$

Two amplitude/phase pairs, for the in-plane and the out-of-plane dynamics, are sufficient to fully characterise a Lissajous orbit. In this work Lissajous have been initialised with equal amplitudes and null phases, $A_x =$

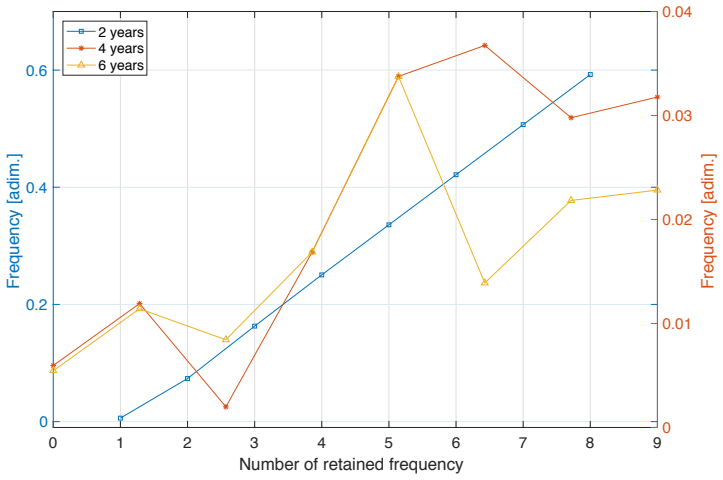

Figure 12: Chosen retained frequencies trend for increasing time domain when extrapolation is performed. The data of the figure corresponds to the refinement of Sun–Earth L_2 halo orbit.

$A_z = 10^{-5}$ (dimensionless units) and $\varphi = \psi = 0$ (see Alessi et al. (2010) for more details).

Fig. 13 displays the refinement of three L_1 Lissajous orbits in three different gravitational systems. The refinement has been carried out for ten primaries complete revolutions; however, only a portion of the trajectories within the RPRnBP is shown for clarity of presentation. The regularity of the refined Lissajous clearly depends on the mass parameter. Indeed, the Sun–Jupiter refined orbit stays very close to its linear counterpart.

The resulting trajectories have been identified to be Lissajous through a Fourier analysis. The main in-plane and out-of-plane frequencies of the refined solutions must match, within a certain threshold, the linear Lissajous frequencies in order to label these orbits as refined Lissajous. Fig. 14 shows the Fourier transform magnitude of the in-plane and out-of-plane motion for the Sun–Jupiter case. Although spurious frequencies appear as result of the gravitational attraction of other celestial bodies, the Lissajous frequencies of the linear CRTBP are retained. Numerical values, listed in Table 3, do not seem to have a predictable trend nor any correlation with the Lissajous Jacobi energy for the tested cases.

All the refined Lissajous trajectories have converged towards slightly smaller amplitudes, and therefore higher Jacobi energy. What is more, the Lissajous trajectories of the Sun–Earth case (second row of Fig. 13) present two anomalies:

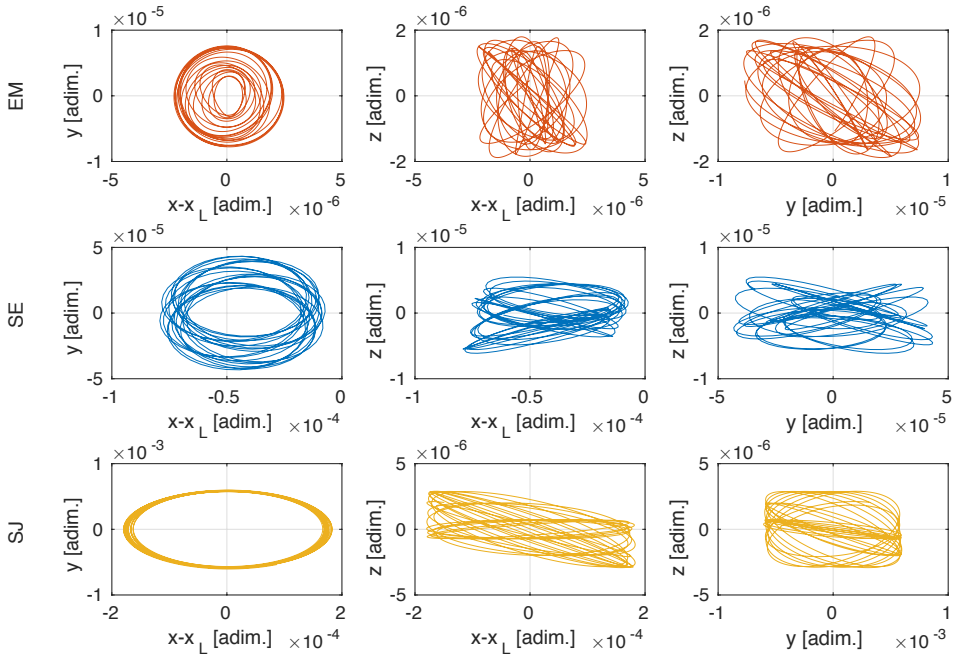

Figure 13: Refinement of L_1 Lissajous orbits for the Earth–Moon (top), Sun–Earth (middle), and Sun–Jupiter system (bottom) in the RPRnBP. For clarity sake, roughly 220 days, 330 days and 95 years of computed orbit are displayed, respectively. The in-plane, A_x, and out-of-plane amplitudes, A_z, are equal to 10^{-5} adimensional units, that is 3.8 Km, 1500 Km, and 7800 Km for the Earth–Moon, Sun–Earth, and Sun–Jupiter systems, respectively.

(i) The frequency corresponding to the largest Fourier transform magnitude coincides with the lunar harmonic motion as seen from the Sun–Earth synodic frame, $f = 1.97477$ (frequency dimensionless units), whereas the Lissajous dynamics stems from the second main frequency;

(ii) The refined Lissajous is actually orbiting around a point that is shifted towards the Sun (in the opposite direction for the L_2 case) with respect to the actual libration point of the Sun–Earth system.

This is true for both L_1 and L_2 refined Lissajous. These effects are conjectured to be caused by the strong perturbation of the Moon on the satellite dynamics along the LPO. This hypothesis is also confirmed by the Fourier analysis, highlighting the major contribution of the Moon.

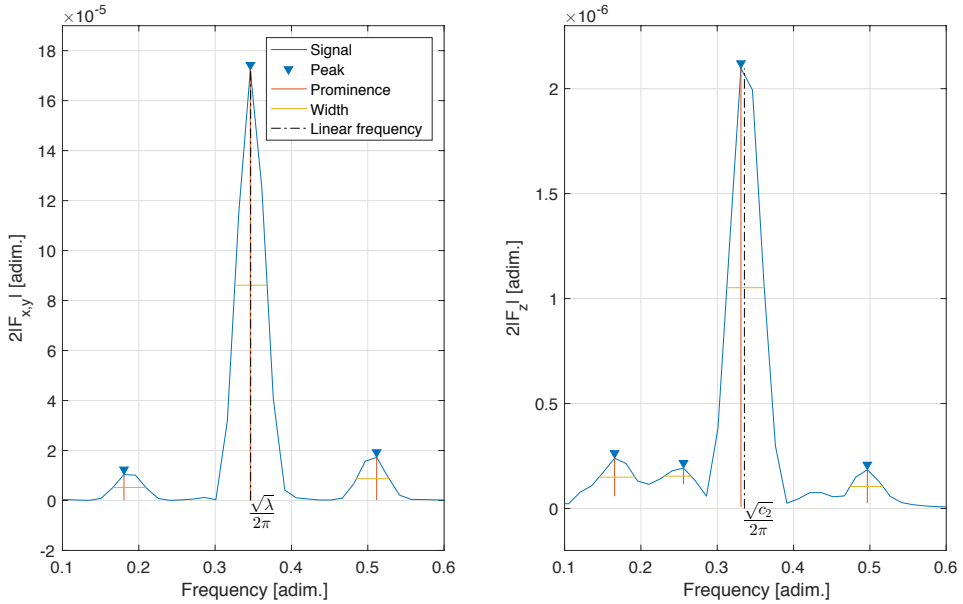

Figure 14: Fourier transform magnitude of the in-plane (left) and out-of-plane (right) motion for the Sun–Jupiter L_1 refined Lissajous orbit. Peaks correspond to the main signal frequencies according to Fourier analysis, while the dashed-dotted black vertical lines correspond to the linear Lissajous frequencies.

Table 3: Difference between the Lissajous linear and refined frequencies for several test cases (primaries and libration point selection).

$\lvert\Delta f\rvert \times 10^{-3}$	EM		SE		SJ	
	L_1	L_2	L_1	L_2	L_1	L_2
x, y	3.71	11.26	1.85	6.70	0.47	22.3
z	0.86	14.10	5.52	3.22	4.52	4.11

4.2.3. The planar Lyapunov family

The planar Lyapunov orbit is located on the xy plane, giving an in-plane motion boundary to the Lissajous orbits. (The vertical Lyapunov orbit, which has zero in-plane motion, sets an out-of-plane limit for the Lissajous ones of the same energy.) In this work, planar Lyapunov orbits are objects of the refinement procedure. In particular, Fig. 15 displays the refinement of two planar Lyapunov orbits emanating from the first libration point, L_1, of Sun–Jupiter system. The seed orbits, calculated in the CRTBP, are characterised by two distinct values of Jacobi constant, that is $C_J = 3.02$ and

$C_J = 3.039$. The iterative procedure has been started (for both orbits) with $\Delta T_0 = 4$, $\Delta T^* = 20$ (unity of measurement is year), and $\gamma_P = 1.3$. With these parameters, 7 iterations are sufficient to reach the final desired time. For either of the two Lyapunov families, orbits with different amplitudes are associated to different energy levels (values of the Jacobi constant); as expected, the orbit with higher C_J has smaller amplitude.

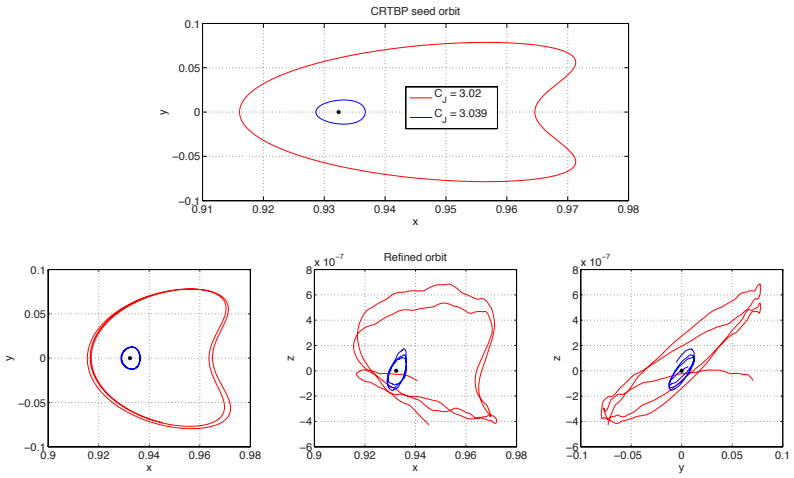

Figure 15: Initial CRTBP guess (top) and 20-year numerical refinement (bottom) of planar Lyapunov orbits with $C_J = 3.039$ (smallest orbit), and $C_J = 3.02$ (largest orbit) of the Sun–Jupiter L_1 libration point (notice the very small z component).

5. Conclusions

In this paper an automatic procedure has been developed, able to refine general trajectories into the real solar system ephemeris model. The transition between simplified and refined trajectory is of essential relevance in the trajectory design phases. The need of having an algorithm capable of this is dual. Firstly, the feasibility assessment of flying such orbits, the transfer navigation analysis, and essentially most of the mission operation phases must be studied, tested and validated in the real solar system dynamics. Secondly, the mission will eventually be flown in the real scenario, thus the nominal trajectory is by definition the one that exists in the real solar system model.

This problem has been studied from an engineering standpoint: the seeding orbits were calculated and designed first in a simplified gravitation model; then they were refined in the n-body problem by means of

the proposed algorithm. Special emphasis has been put in the circular restricted three-body problem, however other simplified models might be used to provide seeding trajectories (e. g., ERTBP or bicircular RFBP). Writing the n-body problem as perturbation of the simpler CRTBP has allowed a convenient and efficient application of a multiple shooting strategy for the refinement procedure. The TPBVB has been transcribed into a parameter optimisation problem and solved as a standard NLP problem, where the dynamics has been viewed as a constraint. The shooting part has been addressed by means of a dedicated parallel computing strategy. Results have been sought for the dynamical substitutes of several three-body systems. Compared to previous works the refinement algorithm features a different approach for the interpolation/extrapolation step and the Fourier analysis. This has shown that the multiple shooting step is able to converge also with a less accurate, from the harmonic content perspective, seeding.

Three different space applicative scenarios have been investigated: the Earth–Moon, the Sun–Earth, and the Sun–Jupiter systems. The latter revealed the easiest to disclose because of its mass preponderance in the solar system, making it minimally affected by perturbations. The analysed cases numerically demonstrate and show that quasi-periodic orbits exist in the neighbourhood of the unstable collinear points in the complete gravitational model. Solutions of the Earth–Moon system have been benchmarked with the ones existing in the present literature. Furthermore, successful application to different gravitational systems has proved the robustness of the algorithm and has displayed how its convergence properties does not depend on the particular mass ratio of the system, thus potentially applicable to a large variety of dynamical problems of this kind.

These orbits can be exploited by a space mission in the real scenario. The results obtained in this work make the algorithm very appealing and potentially applicable for real space applications. Finally, this methodology might also be applied to the refinement of propelled trajectories.

References

Alessi, E.M., Gómez, G., Masdemont, J.J., 2010. Two-manoeuvres transfers between LEOs and Lissajous orbits in the Earth–Moon system. Advances in Space Research 45, 1276–1291. doi:10.1016/j.asr.2009.12.010.

Armellin, R., Topputo, F., 2006. A sixth-order accurate scheme for solving two-point boundary value problems in astrodynamics. Celes-

tial Mechanics and Dynamical Astronomy 96, 289–309. doi:10.1007/s10569-006-9047-4.

Betts, J.T., 2010. Practical methods for optimal control and estimation using nonlinear programming. 2nd ed., Philadelphia, PA : Society for Industrial and Applied Mathematics.

Bolle, A., Circi, C., 2012. A hybrid, self-adjusting search algorithm for optimal space trajectory design. Advances in Space Research 50, 471–488. doi:10.1016/j.asr.2012.04.026.

Dei Tos, D.A., 2014. Automated trajectory refinement of three-body orbits in the real solar system model. Master's thesis. Politecnico di Milano. URL: http://hdl.handle.net/10589/93675.

Folkner, W.M., Williams, J.G., Boggs, D.H., Park, R.S., Kuchynka, P., 2014. The Planetary and Lunar Ephemerides DE430 and DE431. Technical Report. JPL Interplanetary Network Progress Report 42-196.

Gómez, G., Masdemont, J.J., Mondelo, J.M., 2002a. Libration point orbits: a survey from the dynamical point of view. World Scientific. chapter 16. pp. 311–372. doi:10.1142/9789812704849_0016.

Gómez, G., Masdemont, J.J., Mondelo, J.M., 2002b. Solar system models with a selected set of frequencies. Astronomy and Astrophysics 390, 733–750. doi:10.1051/0004-6361:20020625.

Gómez, G., Masdemont, J.J., Mondelo, J.M., 2003. Dynamical substitutes of the libration points for simplified Solar System models. World Scientific. chapter 17. pp. 373–397. doi:10.1142/9789812704849_0017.

Gómez, G., Mondelo, J.M., 2001. The dynamics around the collinear equilibrium points of the RTBP. Physica D: Nonlinear Phenomena 157, 283–321. doi:10.1016/S0167-2789(01)00312-8.

Gómez, G., Mondelo, J.M., Simó, C., 2010a. A collocation method for the numerical fourier analysis of quasi-periodic functions. I: numerical tests and examples. Discrete Contin. Dyn. Syst. Ser. B 14, 41–74. doi:10.3934/dcdsb.2010.14.41.

Gómez, G., Mondelo, J.M., Simó, C., 2010b. A collocation method for the numerical fourier analysis of quasi-periodic functions. II: analytical error estimates. Discrete Contin. Dyn. Syst. Ser. B 14, 75–109. doi:10.3934/dcdsb.2010.14.75.

Gómez, G., Simo, C., Masdemont, J., Jorba, A., 2001. Dynamics and mission design near libration points: Vol. III Advanced methods for collinear points. World Scientific.

Hou, X.Y., Liu, L., 2011. On quasi-periodic motions around the collinear libration points in the real Earth–Moon system. Celestial Mechanics and Dynamical Astronomy 110, 71–98. doi:10.1007/s10569-011-9340-8.

Jorba, A., Masdemont, J., 1999. Dynamics in the center manifold of the collinear points of the restricted three body problem. Physica D: Nonlinear Phenomena 132, 189–213. doi:10.1016/s0167-2789(99)00042-1.

Lian, Y., Gómez, G., Masdemont, J.J., Tang, G., 2013. A note on the dynamics around the Lagrange collinear points of the Earth–Moon system in a complete solar system model. Celestial Mechanics and Dynamical Astronomy 115, 185–211. doi:10.1007/s10569-012-9459-2.

Luo, Z.F., Topputo, F., 2015. Analysis of ballistic capture in Sun–Planet models. Advances in Space Research 56, 1030–1041. doi:10.1016/j.asr.2015.05.042.

Luo, Z.F., Topputo, F., Bernelli-Zazzera, F., Tang, G.J., 2014. Constructing ballistic capture orbits in the real solar system model. Celestial Mechanics and Dynamical Astronomy 120, 433–450. doi:10.1007/s10569-014-9580-5.

Mingotti, G., Topputo, F., Bernelli-Zazzera, F., 2012. Transfers to distant periodic orbits around the Moon via their invariant manifolds. Acta Astronautica 79, 20–32. doi:10.1016/j.actaastro.2012.04.022.

Richardson, D.L., 1980. Analytic construction of periodic orbits about the collinear points. Celestial mechanics 22, 241–253. doi:10.1007/bf01229511.

Shampine, L.F., Reichelt, M.W., 1997. The Matlab ODE suite. SIAM journal on scientific computing 18, 1–22.

Szebehely, V., 1967. Theory of orbits: the restricted problem of three bodies. Academic Press, New York.

Tang, G., Gomez, G., Masdemont, J.J., Yijun, L., et al., 2013. A note on the dynamics around the L1, 2 Lagrange points of the Earth–Moon system in a complete solar system model. Celestial Mechanics and Dynamical Astronomy 15, 185–211. doi:10.1007/s10569-012-9459-2.

Topputo, F., 2013. On optimal two-impulse Earth–Moon transfers in a four-body model. Celestial Mechanics and Dynamical Astronomy 117, 279–313. doi:10.1007/s10569-013-9513-8.

Topputo, F., Belbruno, E., 2015. Earth–Mars transfers with ballistic capture. Celestial Mechanics and Dynamical Astronomy 121, 329–346. doi:10.1007/s10569-015-9605-8.